EFFECT OF FIBRE REINFORCEMENT ON THE CRACK WIDTH PROFILE AND INTERNAL CRACK PATTERN OF CONVENTIONALLY REINFORCED CONCRETE BEAMS

Carlos G. Berrocal[1], Karin Lundgren[2], Ingemar Löfgren[3], Niclas Görander[4] and Christopher Halldén[5]

[1] Industrial PhD Candidate, Chalmers University of Technology and Thomas Concrete Group, Carlos.gil@chalmers.se.
[2] Professor, Chalmers University of Technology, Karin.lundgren@chalmers.se.
[3]Adjunct professor, Chalmers University of Technology, and R&D manager Thomas Concrete Group, Ingemar.lofgren@thomasconcretegroup.com.
[4] M.Sc., Chalmers University of Technology, Niclas.gorander@integra.se,
[5] M.Sc., Chalmers University of Technology, Christopher.hallden@vbk.se

ABSTRACT

Although fibre reinforcement is known to reduce the crack width and crack spacing of conventionally reinforced concrete elements, the impact of fibres on the crack width profile and crack morphology has not received as much attention. This paper presents experimental results of the crack width profile and internal crack pattern obtained from three-point bending test of conventionally reinforced concrete notched beams made of plain concrete and fibre reinforced concrete at low fibre dosages. The induced cracks were, under loaded conditions, injected with a fluorescent epoxy-resin. From each beam, two pieces were extracted and subjected to a second impregnation. Digital images were taken using a microscope and were then processed and analysed to extract quantitative information. The results revealed that the accumulated crack width was similar for all mixes. However, in the samples with fibres the main crack branched off into several narrower cracks compared to plain concrete, which generally exhibited a single and wider crack. Based on the known relation between permeation and crack width, this finding describes a mechanism through which fibre reinforcement can improve the water tightness of reinforced concrete structures and potentially extent their service life reducing the ingress of detrimental agents.

Keywords: steel fibres, hybrid reinforcement, R/FRC, crack morphology, image analysis

Carlos G. Berrocal, Industrial PhD candidate,
Chalmers University of Technology,
Sven Hultins gata 8,
Göteborg, SE-412 58,
Sweden

Email: Carlos.gil@chalmers.se
Tel: +46 317 72 22 62

1. INTRODUCTION

The presence of large cracks in reinforced concrete structures is undesired for various reasons. Large cracks pose an aesthetic issue and the structures might be perceived by the users as unsafe. More importantly, the transport mechanisms that control the ingress of detrimental substances into the concrete may be greatly affected and, consequently, the durability of the structure might be impaired.

The use of fibre reinforcement has been shown to be an effective way to reduce the crack width and crack spacing in conventionally reinforced concrete members. This finding has been consistently observed experimentally through tensile loading of reinforced concrete tie-elements, see e.g. [1–3], in which specimens made of fibre reinforced concrete (FRC) presented narrower and more closely spaced cracks at the surface.

However, the entire crack width profile might be of interest to assess the transport properties of cracked concrete, its autogenous healing capacity, or the cathode-to-anode ratio of macro-cell corrosion. Particularly, the crack width at the reinforcement has been suggested to be a better indicator than surface crack width of the risk of corrosion initiation at the reinforcement [4–6]. Although several studies have looked into the internal profile of cracks in conventionally reinforced elements made of plain concrete, see e.g. [7–9], reinforced elements of fibre reinforced concrete (R/FRC) have received less attention. Moreover, investigations on internal crack profiles have mostly been limited to cracks induced through direct tensile tests in specimens containing high fibre dosages which exhibited strain hardening and multiple cracking [10, 11].

In this paper, the influence of various types of fibre reinforcement at low dosages (< 1% vol.) on the internal crack pattern and crack width profile of reinforced concrete beams subjected to bending loads were investigated. The approach adopted to study the internal cracking of the concrete specimens was image analysis, which has been previously shown to be a suitable tool for the purpose [12, 13]. A combination of techniques reported in the literature were used for the sample preparation, namely crack injection [9, 14] and surface impregnation [12, 15] with fluorescent epoxy resin. Pictures for image analysis were obtained by means of two different acquisition procedures and cracks were measured using a semi-automated algorithm described in [16]. The results here presented include a comparison of the internal crack pattern and measurements of the crack width profile along the concrete cover for the different concrete mixes investigated.

2. EXPERIMENTAL PROGRAM

2.1. Materials and specimens

Three different concrete mixes were used in this investigation to cast a total of twelve beams: (a) plain concrete (PC) beams, without fibre reinforcement; (b) steel fibre reinforced concrete (SFRC) beams, containing 35 mm long low-carbon steel fibres at 0.5% vol.; and (c) hybrid fibre reinforced concrete (HyFRC) beams, featuring a combination of the mentioned steel fibres and micro PolyVinyl-Alcohol (PVA) fibres at 0.5 and 0.15% vol., respectively. All the mixes were self-compacting with a water cement ratio (*w*/c) equal to 0.47. The concrete compositions for the three mixes are shown in Table 1 and the main characteristics of the fibres are presented in Table 2.

The beam specimens had cross-section dimensions of 150·150 mm and a total length of 550 mm. A notch, 10 mm deep, was sawn at the centre of the bottom side of each beam to act as a stress raiser and ensure cracks initiated at that location. Every beam was reinforced with two ∅10 mm ribbed bars with a concrete cover of 60 mm from the bottom face, thus having a clear concrete cover of 50 mm from the notch tip. The specimen geometry and reinforcement layout are schematically presented in Figure 1.

After casting, the specimens were cured in water for three weeks and then cured at 20±2ºC and 60±20% RH for a week prior to cracking. Material tests were carried out to assess the mechanical properties of the concrete mixes. The compressive strength was tested on cubes of 150 mm side length at the age of 28 days in accordance with EN-12390-3 [17] for all mixes whereas the flexural tensile strength was tested for the fibre reinforced mixes, also at 28 days, in accordance with EN-14651 [18].

Table 1. Concrete composition, in kg/m^3

	Concrete mix designation		
Component	PC	SFRC	HyFRC
Cement (CEM I 42.5N SR 3 MH/LA)	360	360	360
Limestone filler (Limus 40)	165	165	165
Fine aggregate (sand 0/4)	776	768	767
Coarse aggregate (crushed 5/16)	840	833	831
Effective water	169	169	169
Superplasticizer – Glenium 51/18	5.76	5.76	5.76
Air entrainer – MicroAir 105	0.36	0.36	0.36
Fibre content (vol. %)	PC	SFRC	HyFRC
Steel – Dramix 65/35-BN	-	0.5	0.5
PVA – Kuralon™ RSC15/8	-	-	0.15

Table 2. Fibre characteristics according to manufacturer specifications

Property	Dramix® 65/35-BN	Kuralon™ RSC15/8
Material	Low carbon steel	Polyvinyl Alcohol
Length [mm]	35	8
Diameter [μm]	550	40
Aspect ratio	65	200
Tensile strength [MPa]	1100	1400
Young's modulus [GPa]	210	35

The average value and standard deviation of the compressive strength obtained for each mix are presented in Figure 2. The average flexural strength vs the crack mouth opening displacement (CMOD) curves for the mixes with fibres are also presented in Figure 2, where residual flexural strength values have been highlighted for selected values of the CMOD.

2.2. Cracking of specimens and epoxy-resin injection of cracks

After curing, the beams were subjected to three-point loading to induce cracking. The cracking procedure aimed at achieving a target crack width at the notch tip rather than a certain load to establish a reference for the comparison of the crack width profile.

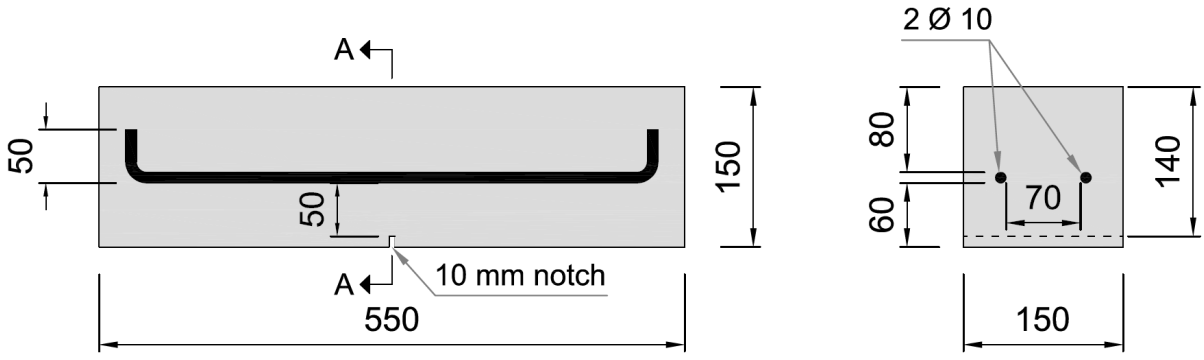

(a) Longitudinal section (b) Cross section (A-A)

Figure 1. Geometry of beam specimens and reinforcement layout.

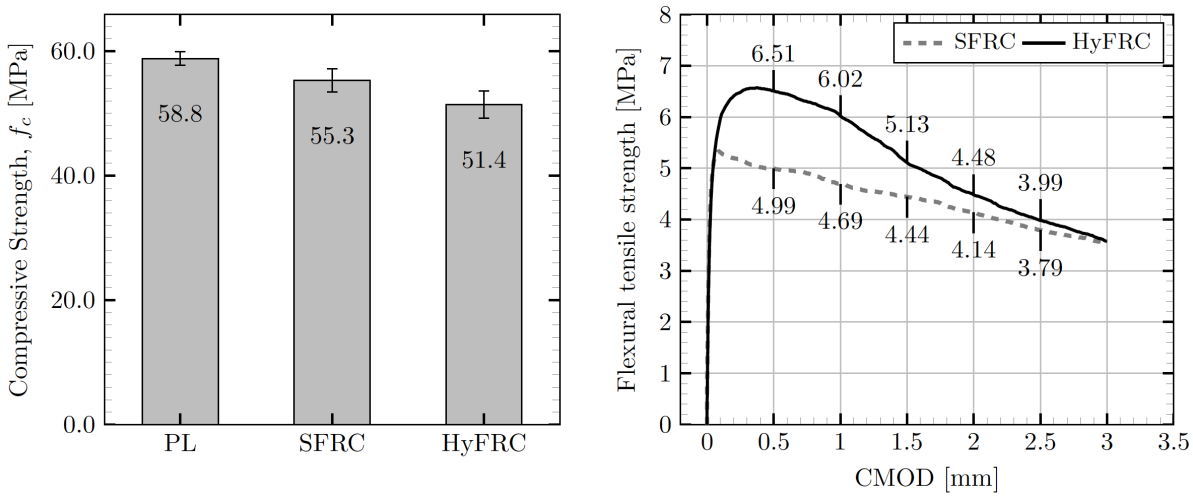

Figure 2. Average compressive strength and flexural tensile strength vs CMOD curves.

Two target crack widths, 0.5 and 1.0 mm, were used in this investigation. It is noteworthy that fibre reinforced beams withstood a load almost 40% greater than their plain concrete counterparts to achieve the same surface crack width.

The cracking procedure was carried out under displacement control at a constant loading rate of approximately 1.5 mm/min. The beams were positioned with the notched side facing upwards, resting on a half-moon support located at the centre of the lower side while the load was introduced by pressing down supports placed at either edge of the beam. During the loading process, a load cell and a clip gauge were used to monitor the load under the central support and the CMOD at the notch. These measurements were used to estimate the target crack width, which was more accurately determined using an optical crack-detection microscope.

Once the target crack width at the notch tip was reached, the displacement of the loading rig was halted to apply a sustained load that would keep the crack open at the aimed width. Subsequently, a low viscosity (0.1 Pa·s) epoxy resin was combined with fluorescent dye and injected into the crack using a syringe. The cracks on the lateral sides of the beams were sealed using hot-melt adhesive to prevent leakage of the resin, which was continuously added until the crack was completely filled. The epoxy resin was then left to harden and cure for at least 16 hours before removing the load to avoid having crack re-closing. The process is schematically illustrated in Figure 3.

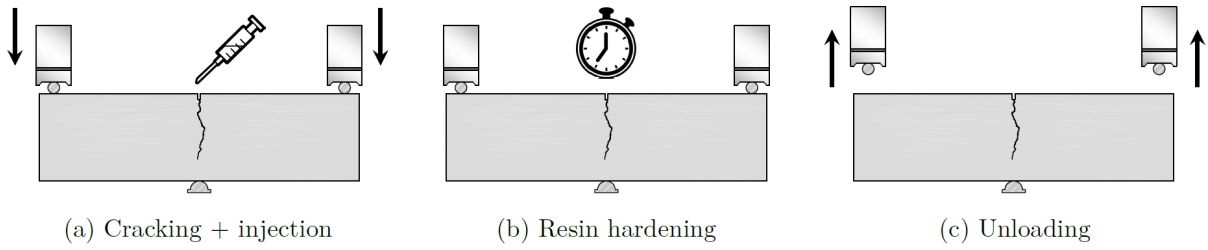

Figure 3. Inverted three point loading setup for cracking and injection procedure of epoxy resin.

2.3. Preparation and vacuum impregnation of crack samples

Since cracks are particularly relevant for the ingress of external agents into the concrete, which can be detrimental for the reinforcement, the crack width profile was of special interest at the reinforcement sections. Consequently, after the injected resin had hardened, the beams were sawn to obtain two crack specimens out of each beam. First, the central 200 mm of the beam were sawn by performing two transverse cuts and after that two more cuts were performed parallel to the reinforcement to obtain the crack specimens exhibiting the sought crack profile, see Figure 4.

Although the resin had successfully filled the main crack, some of the secondary cracks visible at the surface of the specimens could not be completely filled during the injection procedure. In order to fill these cracks with fluorescent resin as well, the samples were subjected to a vacuum impregnation process. The vacuum impregnation was followed by grinding of the surface to remove the excess of resin as well as to provide a flat, smooth surface, suitable for microscopy. The relative position of the crack specimens within the beam and the resulting appearance of the specimens after vacuum impregnation and grinding are presented in Figure 4.

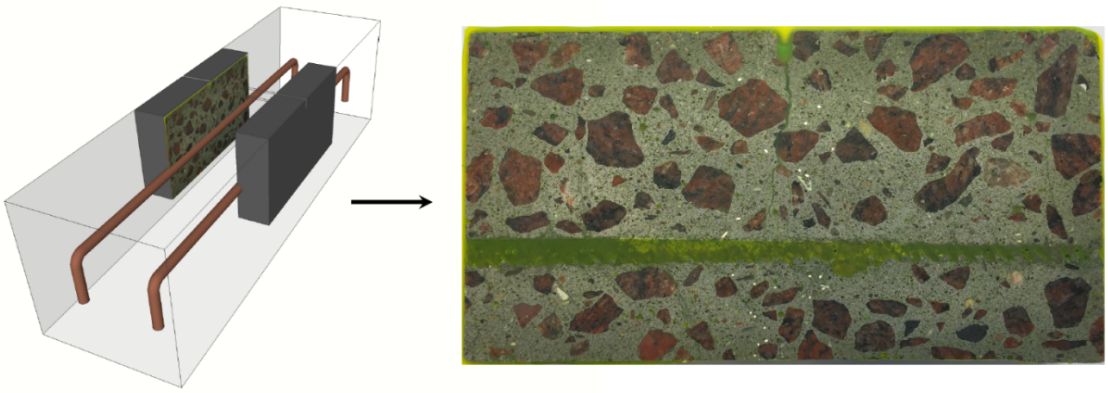

Figure 4. Schematic representation of sections of the beam analyzed and final result after sample preparation.

3. IMAGE ANALYSIS

3.1. Acquisition of images

Two different approaches were adopted to perform image acquisition, photography under ultra violet (UV) light and microscopy under normal light. A digital camera and two lamps with UV-emitting light bulbs were used for the first approach to take pictures of the entire crack length, at a resolution of 3072·4080 pixels (25μm/pixel). A microscope outfitted with a digital camera was used in the second approach to acquire multiple partial images of the crack, taken at a 20· magnification and a resolution of 2583·1936 pixels (2.7 μm/pixel), which were later automatically assembled using a AxioVision software to obtain a full picture of the crack.

Each of the approaches described had its own advantages. Thanks to the fluorescent dye mixed in the resin, images taken under UV light provided an excellent contrast between the impregnated cracks and the background (matrix and aggregates), facilitating the processing of the images. On the other hand, the images taken with the microscope provided a much higher resolution of the crack, thus increasing the precision of the crack measurements. An example of the images obtained using both approaches is presented in Figure 5 for the same crack to illustrate the advantages of each approach.

3.2. Image processing

Processing of the images was necessary in order to extract the desired features of the original colour images and obtain a binary (black and white) image, suitable for analysis purposes. As earlier stated, the main advantage of using images taken under UV light is the high contrast between the impregnated regions and the background, but also the colour uniformity throughout the entire crack surface. This feature enabled a thresholding of the image based solely on the colour intensity of the green channel. Pictures taken under normal light conditions required a more elaborated process, working in the HSB (Hue, Saturation, Brightness) to perform the thresholding operation. After thresholding, binary images were cleaned and filtered to remove background noise and to smoothen the crack edges. In Figure 5, processed binary images are displayed beside their corresponding colour image.

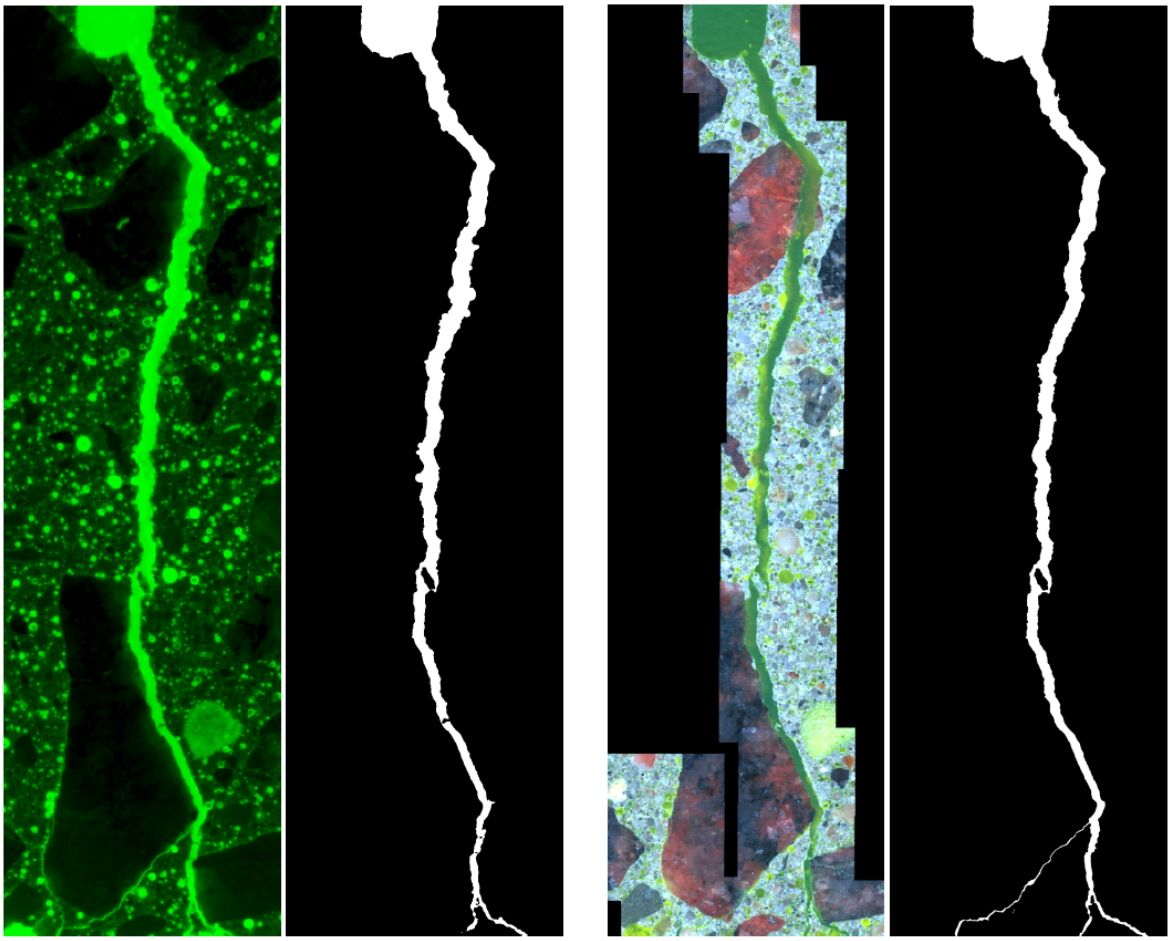

(a) UV light conditions (b) Normal light conditions

Figure 5. Original and processed images for two different image acquisition approaches.

3.3. Determination and measurement of the crack width

Cracks in concrete often present a highly irregular morphology and deciding how the crack width should be determined is not always straightforward. The degree of tortuosity of a crack may be dependent on various reasons, e.g. the presence of aggregates along the crack path or the concrete strength among others, and therefore crack tortuosity in concrete may vary significantly. In some cases, cracks propagate describing a pseudo-straight trajectory and the crack width can be roughly determined as the width measured perpendicularly to the global direction of propagation. This approach was adopted e.g. by Qi et al. [13], who investigated plastic shrinkage cracks formed along a stress raiser on slab elements.

Using the global direction of propagation to measure the crack width implies that as soon as the crack deviates from that direction an error is introduced in the measurement, which increases as the angle of deviation increases. Fibres, as aggregates, might interfere with the crack morphology causing it to change direction or split, potentially increasing tortuosity. Consequently, an approach in which the crack width is measured perpendicularly to the local direction of propagation would be preferable.

In order to quantify the crack width, an algorithm based on the arc-length concept was implemented in Matlab® to find points along the centreline of the crack. Then, the crack width was computed as twice the minimum distance between each point and the crack edge. When several cracks were present at the same cover depth, the crack width of all cracks was determined individually based on the aforementioned procedure. Subsequently, the maximum individual crack width and the accumulated crack width, an equivalent crack width equal to the sum of each individual crack, were determined for each cover depth. The crack width measurement procedure is schematically presented in Figure 6.

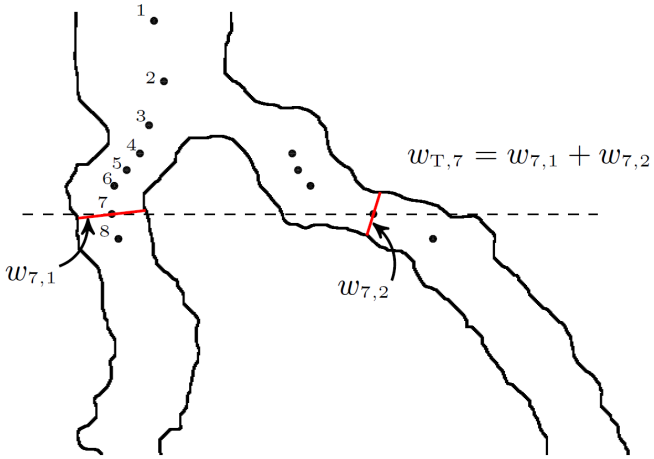

Figure 6. Schematic representation of the procedure used to determine the crack width at each depth level.

Additionally, in order to assess the accuracy of the algorithm developed, the crack width was manually measured. Using the scale information of the digital images taken with a microscope, the crack width was evaluated at 2 mm intervals with AxioVision software built-in tools.

4. RESULTS AND DISCUSSION

4.1. Image acquisition techniques

The acquisition of images plays a key role when using image analysis. An example of its importance can be observed in Figure 5. Although both processed images were naturally alike, two dissimilarities attributable to the thresholding operation could be noticed. The most obvious was the absence of a thin crack near the bottom of the fluorescent binary image. Subtler yet noticeable, the binary fluorescent image presented rougher and more irregular edges than the binary image of the crack under normal light conditions.

As mentioned earlier, due to the colour uniformity of the fluorescent images, thresholding was based only on the colour intensity. Consequently, all elements featuring an intensity below the selected threshold, including thin cracks, were not incorporated into the binary image. On the other hand, small defects along the crack path such as air voids, which were filled with resin during the vacuum impregnation, could not be isolated from the cracks and were included in the binary image. Whereas smaller cracks could be detected by reducing the threshold value, this action would likely worsen the overall image as more defects would be included.

An additional issue was detected concerning the fluorescent images when analysing cracks. While the crack width measured with the algorithm on normal light images showed good agreement with manually measured crack widths, a generalised overestimation of the crack width in fluorescent images was detected, which is illustrated in Figure 7. This outcome indicated that the concentration of fluorescent dye added to the epoxy resin should have been calibrated with the UV lamps employed to prevent the excessive glow of the resin.

4.2. Crack pattern

A significant variation in the crack pattern was observed among the different concrete mixes. Three images representative of the different crack patterns found are presented in Figure 8.

Plain concrete specimens generally exhibited a single wider crack propagating through the whole concrete cover and secondary cracks appeared almost exclusively near the reinforcement. These secondary cracks seemed to initiate at the reinforcement lugs and propagated diagonally towards the main crack, which is indicative of bond-stress cracks as described by Goto [8].

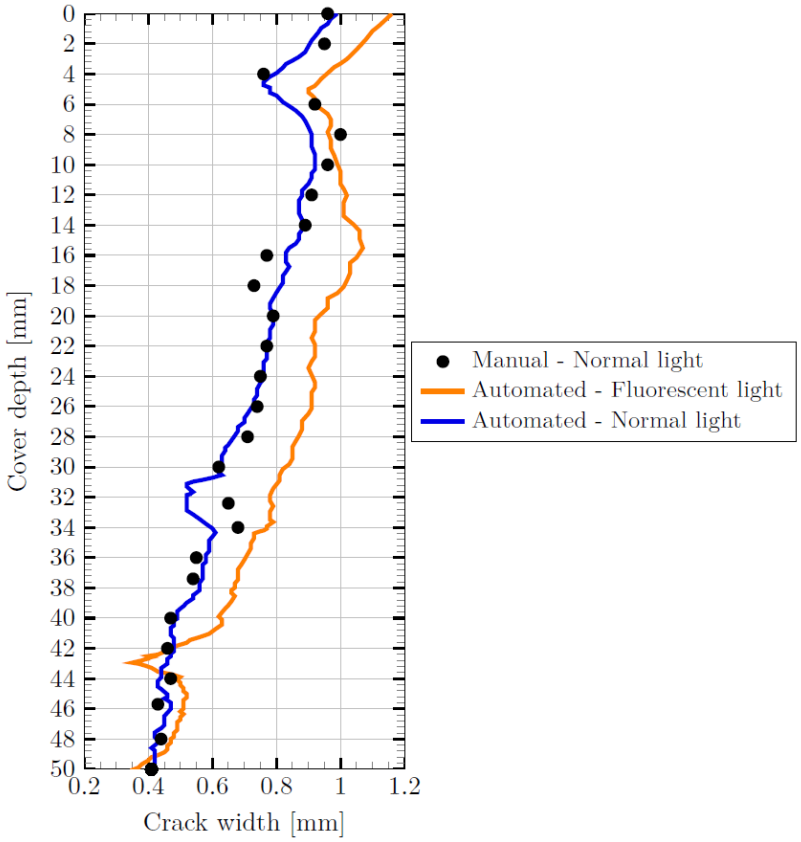

Figure 7. Comparison of the crack width profile measured using different methods.

Specimens with steel fibres usually showed a main crack propagating through the whole cover, often accompanied by secondary cracks propagating parallel to the main crack (approximately in 50% of the cracks analysed). When secondary cracks were present, they generally appeared in the bottom half or in the vicinity of the notch and were continuous and well-defined.

Finally, specimens reinforced with a blend of steel and micro-PVA fibres exhibited a more intricate pattern, where cracks usually branched out creating systems of numerous thinner cracks with complex geometries, appearing along the entire crack length.

4.3. Accumulated crack width

Figure 9(a) presents the accumulated crack width measured at the notch tip as a function of the accumulated crack width at the reinforcement level. As observed, the measured crack widths at the notch tip differ slightly from the target values of 0.5 and 1.0 mm, regardless of the concrete mix. Since cracks were monitored at the external lateral sides of the beams during the loading procedure, that difference can be attributed to the expected variation of the crack width along the surface crack length.

The average ratio between the accumulated crack width at the notch tip and at the reinforcement is presented in Figure 9(b). Based on this ratio, the crack width at the reinforcement did not seem to be influenced by the surface crack width as no clear correlation could be observed between the two cases studied. Furthermore, the variation of the ratio could not be attributed to the presence of fibres either since the differences found were much lower than the scatter presented throughout individual measurements, scatter that increased in fibre reinforced specimens. This finding, however, might be partly attributed to the particular geometry of the beams, in which the concrete cover represented a significant percentage of the total cross-sectional height.

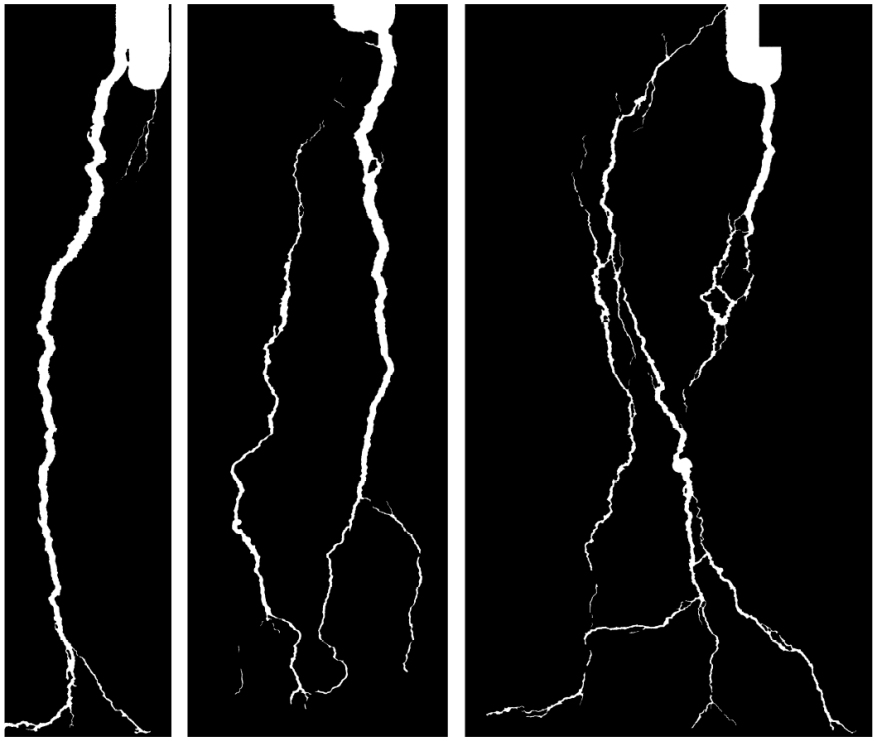

(a) PL (b) SFRC (c) HyFRC

Figure 8. Representative examples of the crack pattern observed for the different concrete mixes studied.

Nevertheless, it should be noted that fibre reinforced specimens required substantially greater loads than plain concrete specimens to achieve a similar crack width at the notch. Had the load been kept at the same level, the crack widths of fibre reinforced specimens would have been a mere fraction of the cracks measured in plain concrete specimens. Moreover, the results indicating that the accumulated crack width profile is not affected by the addition of fibres, added to the higher tendency of cracks to branch out in the presence of fibres as seen in the crack patterns presented in Figure 8, support the observation that cracks propagating in fibre reinforced concrete mixes are, indeed, narrower than cracks formed in plain concrete for the same surface crack width. This outcome may have positive implications regarding the permeation of cracked concrete based on Poiseuille's law, which relates the water flow through a crack to the cube of the crack width, as discussed by Akhavan et al. [19].

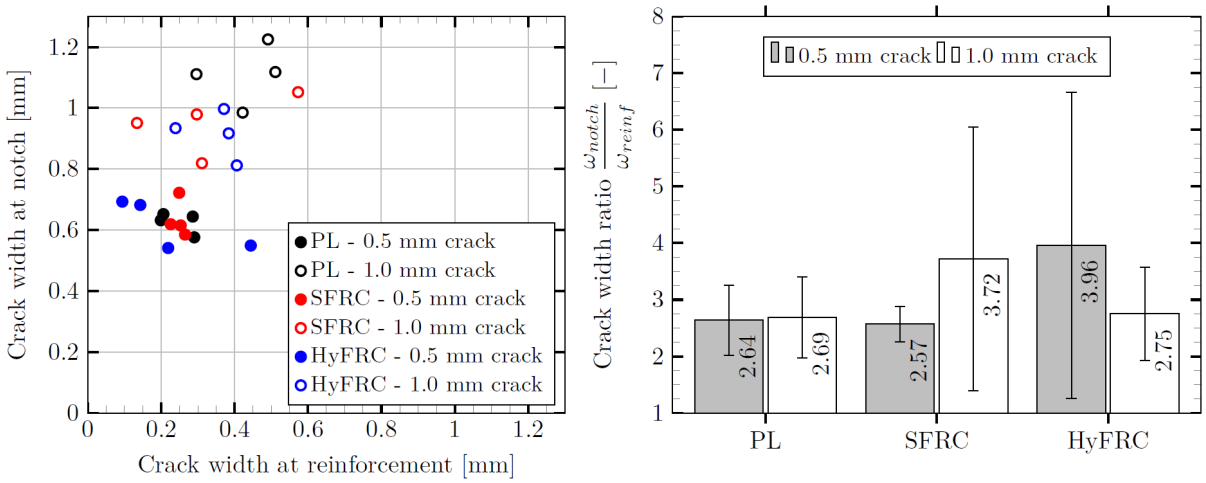

Figure 9. (a) Crack width at the reinforcement vs crack width at the notch (accumulated) and (b) average crack width ratio and standard deviation for the different mixes and loading cases.

4.4. Maximum crack width

Despite exhibiting a nearly constant reduction of the accumulated crack width, the number of secondary cracks increased in the specimens containing fibres, resulting in narrower cracks. As discussed by Edvardsen [20], narrow cracks favor autogenous healing caused by various reasons such as the continued hydration of the cement paste, the precipitation of $CaCO_3$ crystals or blocking of the flow path by impurities among others. According to Edvarsen, for a given hydraulic gradient, a critical crack width exist below which autogenous healing can be achieved.

The maximum individual crack width along the cover depth was measured for each specimen studied. In figure 10, these values are presented together with an average maximum crack width. For the purpose of comparison and in line with the concept autogenous healing crack limitation, the crack length featuring an average maximum crack width below certain reference values, namely 0.2, 0.3 and 0.4 mm have been highlighted in Figure 10.

As observed, only about 1% of the crack length was below a width of 0.2 mm for PC specimens, while this ratio increased to 12% and 20% for SFRC and HyFRC, respectively. This difference between mixes was, however, relatively lower when comparing the crack length featuring a width below 0.3 mm (20% PC, 42% SFRC, 41% HyFRC) and was further reduced for a width of 0.4 mm (52% PC, 56% SFRC, 58% HyFRC). These results suggest that adding fibre reinforcement might contribute to increase the autogenous healing capability of concrete elements with flexural cracks.

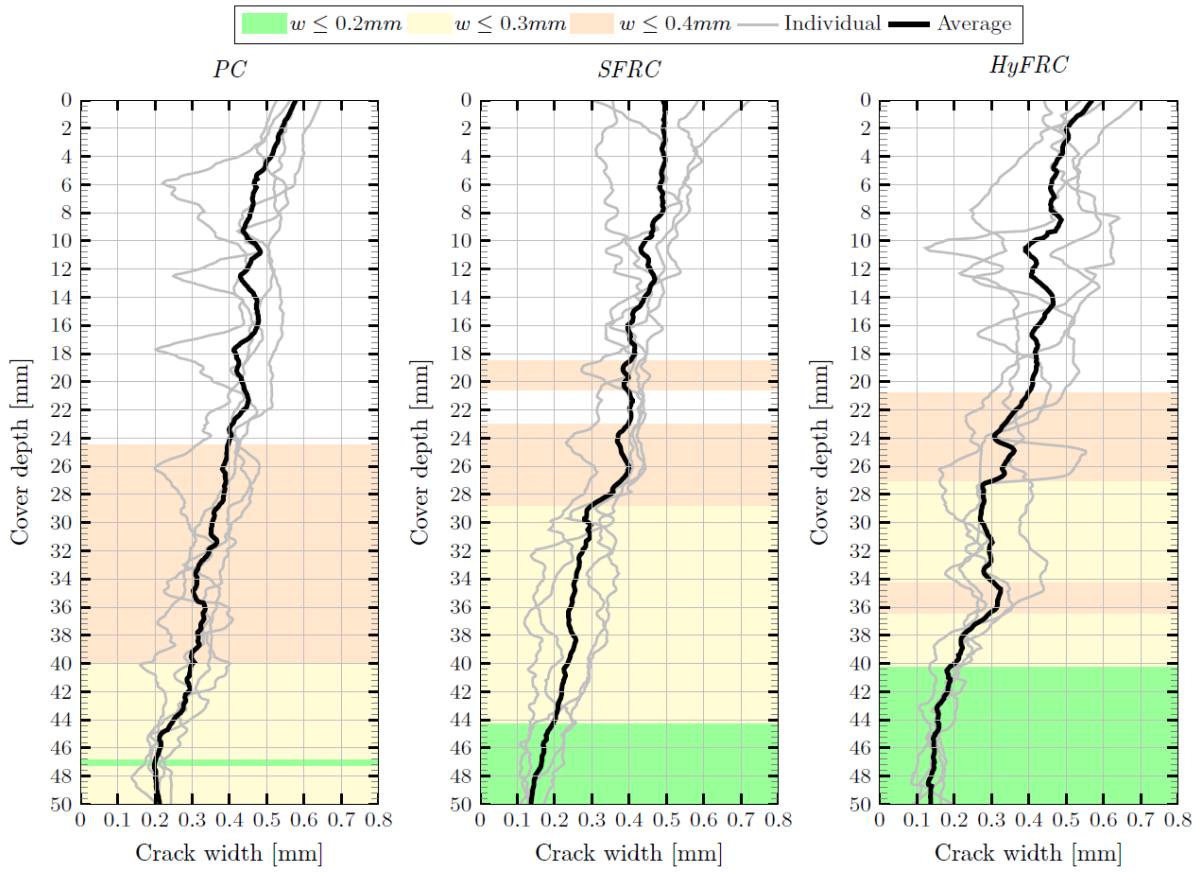

Figure 10. Individual and average maximum crack width. Shaded regions represent where the crack width is below the corresponding value in the legend.

5. CONCLUSIONS

In this paper, the influence of fibre reinforcement on the crack width profile and crack pattern of conventionally reinforced concrete beams subjected to bending was investigated by image analysis.

The procedure developed for image processing in order to determine the internal crack morphology and measure crack widths, including inverted loading of beams, injection of cracks with resin and vacuum impregnation of sawn specimens, proved to be useful and permitted a quantitative determination of important crack features.

The image acquisition procedure was found to be determinant for the crack morphology analysis. Crack pictures taken under UV light facilitated the image processing operations, although the results revealed that a mismatch between the concentration of fluorescent dye and the intensity of the UV lamps can lead to excessive glow and, consequently, overestimation of the crack width. Images taken with microscope under normal light required a more laborious processing but yielded results that are more accurate. Ideally, a microscope outfitted with UV emitting light should provide a higher accuracy to processing time ratio.

The crack pattern underwent a distinctive change as fibre reinforcement was incorporated into the mix. Plain concrete specimens generally exhibited a wide single crack whereas in fibre reinforced specimens the initial crack formed at the notch branched out into two or more cracks as it propagated towards the reinforcement.

Analysis of the crack width revealed that fibres did not significantly influence the accumulated crack width profile along the concrete cover whereas the average surface to reinforcement crack width ratio was found to be independent of the crack width reached at the surface. However, as a consequence of the multiple crack branching, cracks in fibre reinforced concrete specimens were narrower. These findings, added to additional load needed to achieve a similar surface crack width in fibre reinforced beams, suggests that fibre reinforcement may decrease concrete permeation and contribute to crack autogenous healing in reinforced concrete members with bending cracks, thereby potentially improving their durability.

ACKNOWLEDGMENTS

The authors greatly acknowledge the financial support of Thomas Concrete Group. The authors want to thank The Swedish Cement and Concrete Research Institute (CBI), and particularly Dr. Jan Erik Lindqvist, for providing access to their equipment and for assisting with the preparation procedure of the specimens used in this investigation.

REFERENCES

1. Abrishami, H., & Mitchell, D. (1997). Influence of steel fibers on tension stiffening. *ACI structural journal*, *94*, 769–776.
2. Bischoff, P. H. (2003). Tension Stiffening and Cracking of Steel Fiber-Reinforced Concrete. *Journal of Materials in Civil Engineering*, *15*(2), 174–182. doi:10.1061/(ASCE)0899-1561(2003)15:2(174)
3. Jansson, A., Flansbjer, M., Löfgren, I., Lundgren, K., & Gylltoft, K. (2012). Experimental investigation of surface crack initiation, propagation and tension stiffening in self-compacting steel-fibre-reinforced concrete. *Materials and Structures*, *45*(8), 1127–1143. doi:10.1617/s11527-012-9821-6
4. Pease, B., Geiker, M., Stang, H., & Weiss, J. (2010). The design of an instrumented rebar for assessment of corrosion in cracked reinforced concrete. *Materials and Structures*, *44*(7), 1259–1271. doi:10.1617/s11527-010-9698-1
5. Silva, N. (2013). *Chloride Induced Corrosion of Reinforcement Steel in Concrete. Threshold*

Values and Ion Distributions at the Concrete-Steel Interface. Chalmers University of Technology, Gothenburg, Sweden.

6. Michel, A., Solgaard, A. O. S., Pease, B. J., Geiker, M. R., Stang, H., & Olesen, J. F. (2013). Experimental investigation of the relation between damage at the concrete-steel interface and initiation of reinforcement corrosion in plain and fibre reinforced concrete. *Corrosion Science*, *77*, 308–321. doi:10.1016/j.corsci.2013.08.019
7. Broms, B. B. (1965). Crack Width and Crack Spacing in Reinforced Concrete Members. *ACI Journal Proceedings*, *62*(10), 1237–1256.
8. Goto, Y. (1971). Cracks Formed in Concrete Around Deformed Tension Bars. *ACI Journal Proceedings*, *68*(4), 244–251. doi:10.14359/11325
9. Husain, S., & Ferguson, P. M. (1968). *Flexural Crack Width at the Bars in Reinforced Concrete Beams*. Austin, Texas.
10. Otsuka, K., Mihashi, H., Kiyota, M., Mori, S., & Kawamata, A. (2003). Observation of Multiple Cracking in Hybrid FRCC at Micro and Meso Levels. *Journal of Advanced Concrete Technology*, *1*(3), 291–298. doi:10.3151/jact.1.291
11. Lárusson, L. H. (2013). *Development of Flexible Link Slabs using Ductile Fiber Reinforced Concrete*. Technical University of Denmark, Lyngby, Denmark.
12. Ammouche, A., Riss, J., Breysse, D., & Marchand, J. (2001). Image analysis for the automated study of microcracks in concrete. *Cement and Concrete Composites*, *23*(2-3), 267–278. doi:10.1016/S0958-9465(00)00054-8
13. Qi, C., Weiss, J., & Olek, J. (2003). Characterization of plastic shrinkage cracking in fiber reinforced concrete using image analysis and a modified Weibull function. *Materials and Structures*, *36*(July), 386–395.
14. Illston, J. M., & Stevens, R. F. (1972). Long-Term Cracking in Reinforced Concrete Beams. *Proceedings of the Institution of Civil Engineers*, *53*, 445–459.
15. Hornain, H., Marchand, J., Ammouche, A., Commène, J. P., & Moranville, M. (1996). Microscopic Observation of Cracks in Concrete - A new sample preparation technique using dye impregnation. *Cement and Concrete Research*, *26*(4), 573–583.
16. Berrocal, C. G., Löfgren, I., Lundgren, K., Görander, N., & Halldén, C. (2016). Characterisation of bending cracks in R/FRC using image analysis. Submitted to "Cement and Concrete Research."
17. EN 12390-3:2009 Testing hardened concrete. Part 3: Compressive strength of test specimens. (2009).
18. EN 14651:2007 Test method for metallic fibered concrete - Measuring the flexural tensile strength (limit of proportionality (LOP), residual). (2007). Brussels, Belgium.
19. Akhavan, A., Shafaatian, S.-M.-H., & Rajabipour, F. (2012). Quantifying the effects of crack width, tortuosity, and roughness on water permeability of cracked mortars. *Cement and Concrete Research*, *42*(2), 313–320. doi:10.1016/j.cemconres.2011.10.002
20. Edvardsen, C. (1999). Water Permeability and Autogenous Healing of Cracks in Concrete. *ACI Materials Journal*, *96*(4), 448–455.